Magnetic Resonance in Medicine 51:81–92 (2004)

Time-Optimal Multidimensional Gradient Waveform Design for Rapid Imaging

Brian A. Hargreaves,* Dwight G. Nishimura, and Steven M. Conolly

Magnetic resonance imaging (MRI) is limited in many cases by long scan times and low spatial resolution. Recent advances in gradient systems hardware allow very rapid imaging sequences, such as steady-state free precession (SSFP), which has repetition times (TRs) of 2–5 ms. The design of these rapid sequences demands time-optimal preparatory gradient waveforms to provide maximum readout duty-cycle, and preserve spatial resolution and SNR while keeping TRs low. Time-optimal gradient waveforms can be synthesized analytically for certain simple cases. However, certain problems, such as time-optimal 2D and 3D gradient design with moment constraints, either may not have a solution or must be solved numerically. We show that time-optimal gradient design is a convex-optimization problem, for which very efficient solution methods exist. These methods can be applied to solve gradient design problems for oblique gradient design, spiral imaging, and flow-encoding using either a constant slew rate or the more exact voltage-limited gradient models. Ultimately, these methods provide a time-optimal solution to many 2D and 3D gradient design problems in a sufficiently short time for interactive imaging. Magn Reson Med 51:81–92, 2004. © 2003 Wiley-Liss, Inc.

Key words: linear programming; gradient; rapid imaging; spiral; moment-nulling

Scan times in magnetic resonance imaging (MRI) are generally limited by either the signal-to-noise ratio (SNR) or the gradient amplitude and speed. SNR limitations are being met by advances in higher-field systems, as well as improved receive coils. Additionally, many advances are being made in gradient systems to allow rapid imaging with high spatial resolution. These advances include increased switching rates and gradient amplitudes. Also, as the demand for continuous rapid imaging increases, gradient amplifiers are being made more resilient to heating limitations. Acquisition and reconstruction hardware has also improved in response to the development of parallel and real-time imaging techniques.

These advances in MR system hardware have enabled the use of new rapid pulse sequences. Typical rapid sequences include rapid gradient-echo (fast low-angle shot (FLASH), gradient-recalled acquisition in steady state (GRASS)) (1), and multi-echo spin-echo (e.g., turbo spin-echo (TSE), fast spin-echo (FSE), and rapid acquisition with relaxation enhancement (RARE)) sequences (2). Refocused steady-state free precession (SSFP), fast imaging with steady precession (True-FISP), fast imaging employing steady-state acquisition (FIESTA), and balanced-FFE sequences (3,4), which produce high signal and contrast, are becoming common as improved gradients allow imaging with minimal artifacts from off-resonance. All of these sequences demand efficient gradient waveform design. Efficient acquisition methods include echo-planar imaging (EPI) (5) and spiral imaging (6). Aside from imaging trajectories, gradient waveform design includes preparatory waveforms such as phase-encoding, prewinder, and rewinder gradients. In rapid sequences with short repetition times (TRs), the design of these latter gradients is an important consideration for improving imaging efficiency, because their duration reduces the image acquisition duty cycle.

In particular, the design challenge is to minimize gradient waveform durations subject to both hardware constraints and sequence constraints, such as the desired gradient area. Numerous previous works have presented different methods to optimize gradients in different situations (7–14). Many of these methods are limited to the design of trapezoidal pulses, and most have been demonstrated for 1D gradient design. Simonetti et al. (7,8) presented a general technique to minimize 1D-gradient properties (such as moments, diffusion-sensitivity, and RMS-current of 1D gradients) using numerical optimization. Here we expand that work to the design of minimum-time 2D and 3D gradient waveforms subject to pulse sequence and hardware constraints. We demonstrate the power of this technique in producing the time-optimal preparatory gradients for freely-rotatable scans (such as rapid spiral imaging), including higher-moment-nulled trajectories.

The design method can be used to design minimum-time gradient waveforms that satisfy gradient amplifier current and voltage limitations. Additional constraints, such as gradient start and end amplitudes, gradient area, and higher-order gradient moments, can be included. Most importantly, this method can be applied to multidimensional gradient design, which is necessary for moment-nulled spiral trajectory design. Our methods offer a time-optimal solution to numerous problems for which no other time-optimal solution is known.

THEORY

We begin by describing the general constraints involved in gradient waveform design, including gradient amplifier voltage and current limits, and pulse-sequence requirements. Next we describe ways to formulate a problem so that it can be solved using three different types of existing linear and quadratic programming techniques. All of these techniques result in comparable solutions, but the convergence speed and the availability of the software can vary.

Magnetic Resonance Systems Research Laboratory, Department of Electrical Engineering, Stanford University, Stanford, California.

Grant sponsor: NIH; Grant numbers: HL39297; HL56394; AR46904; CA50948; EB000346; EB000777-01; Grant sponsor: State of California; Grant number: TRDRP 9RT-0024; Grant sponsor: GE Medical Systems.

*Correspondence to: Brian A. Hargreaves, Room 212, Packard Electrical Engineering Bldg., Stanford University, Stanford, CA 94305-9510. E-mail: brian@mrsrl.stanford.edu

Received 14 May 2003; revised 27 August 2003; accepted 27 August 2003.
DOI 10.1002/mrm.10666
Published online in Wiley InterScience (www.interscience.wiley.com).

Physical Constraints

A gradient amplifier supplies current to a gradient coil, producing a continuously varying gradient, $G(t)$. The amplifier has current and voltage limits (I_{max} and V_{max}) that result in the following limits on $G(t)$, as described in Refs. 15 and 16:

$$|G(t)| \le \eta I_{max} \quad [1]$$

$$\left| L \frac{d}{dt} G(t) + RG(t) \right| \le \eta V_{max} \quad [2]$$

Here L, R, and η are the gradient coil inductance, resistance, and efficiency (in mT/m/A). In MRI systems, the gradient can be considered a vector, $\vec{G}(t)$ that is composed of three components, $G_x(t)$, $G_y(t)$, and $G_z(t)$. The primary purpose of this work is to specify gradient waveforms that can be freely rotated in three dimensions. This constrains the maximum gradient or change of gradient in any direction, and the constraints of Eqs. [1] and [2] become (with $G_{max} = \eta I_{max}$):

$$\|\vec{G}(t)\|_2 \le G_{max} \quad [3]$$

$$\left\| L \frac{d}{dt} \vec{G}(t) + R\vec{G}(t) \right\|_2 \le \eta V_{max} \quad [4]$$

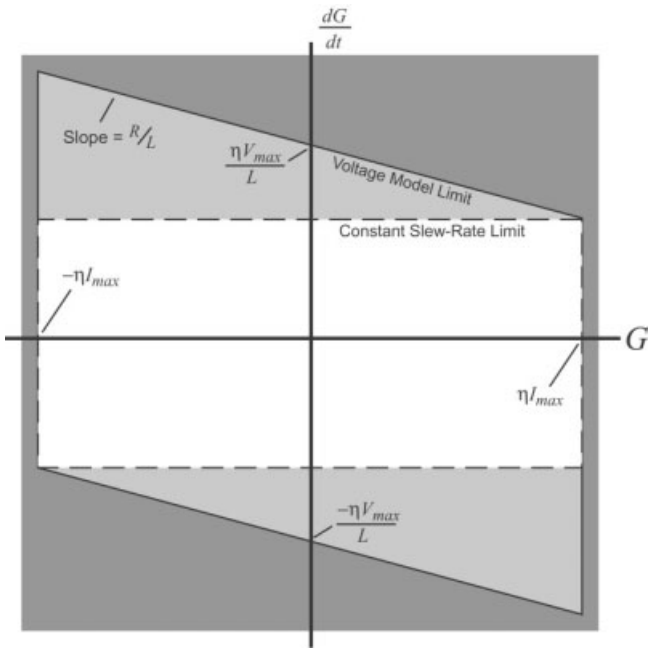

FIG. 1. Limits on gradient amplitude and slew rate for a single-axis gradient due to maximum current (I_{max}) and maximum voltage (V_{max}). Limits are shown using the common constant-slew-rate-limit model (white area) and the more accurate voltage-limit model (white plus light gray areas). As the ratio of coil resistance (R) to coil inductance (L) increases, the constant-slew-rate model becomes increasingly constraining, and the voltage-limit model should be used. η is the ratio of gradient strength to gradient coil current.

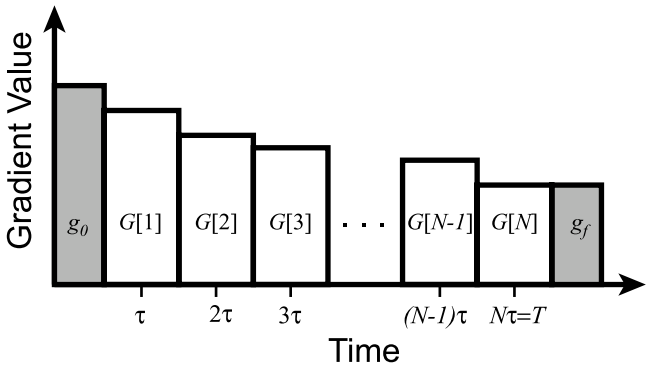

FIG. 2. A gradient waveform can be approximated as a sequence of discrete rectangles that have height $G[n]$ and are centered at times $n\tau$.

where $\|\vec{G}(t)\|_2 = \sqrt{G_x(t)^2 + G_y(t)^2 + G_z(t)^2}$ is the 2-norm (or magnitude) of the gradient vector, $\vec{G}(t)$. Frequently, a simpler "constant-slew-rate-limit" model is used, where ηRI_{max} is subtracted from the right-hand side of Eqs. [2] and [4], and the $RG(t)$ or $R\vec{G}(t)$ term is omitted. For a single gradient axis, the constraints of the voltage model and the constant-slew-rate-limit model are shown in Fig. 1. As the ratio of coil resistance to coil inductance increases, the constant-slew-rate-limit model becomes more constraining.

Pulse Sequence Constraints

Imaging requirements of the pulse sequence constrain the k-space change ($\Delta\vec{k}$) that the gradients will produce over a time interval $[0,T]$ as

$$\int_{t=0}^{T} \vec{G}(t)dt = \frac{2\pi}{\gamma} \Delta\vec{k} \quad [5]$$

Additionally, there are cases in which higher-order moments of the gradients can be specified as

$$\int_{t=0}^{T} t^q \vec{G}(t)dt = \frac{2\pi}{\gamma} \Delta\vec{m}_q \quad [6]$$

where $\Delta\vec{m}_q$ is a specified design constraint on the change in the q^{th} moment of the gradient.

The boundary constraints on the gradient waveforms include having specified initial and final values for the gradient, i.e., $\vec{G}(0) = \vec{g}_0$ and $\vec{G}(T) = \vec{g}_f$. This is necessary to design gradient waveforms at the start and end of the sequence, and to link different waveforms together.

Discrete-Time Gradient Design

Practical gradients are generated as discrete-time waveforms with a sampling period τ. We represent a gradient waveform as a discrete sequence $\vec{G}[n] = \vec{G}(n\tau)$ with $n = 1 \ldots N$. Figure 2 shows a single component of the discrete-time vector $\vec{G}[n]$. The constraints in Eqs. [1]–[6] can easily

be converted to discrete-time equivalents, where a derivative is approximated by the slope between two consecutive samples, and an integral is approximated by a discrete sum multiplied by τ. Specifically, it is useful to express the voltage constraint (Eq. [4]) as

$$\|\alpha\vec{G}[n] + \beta\vec{G}[n+1]\|_2 \leq \psi \qquad [7]$$

where $\alpha = R - \frac{L}{\tau}$, $\beta = \frac{L}{\tau}$, and $\psi = \eta V_{max}$ for the voltage model. In the constant-slew-rate-limit model, $\alpha = -\frac{L}{\tau}$, $\beta = \frac{L}{\tau}$, and $\psi = \eta(V_{max} - RI_{max})$.

Expansion to Multiple Dimensions

There are numerous cases in which gradients must be designed in a 2D or 3D space that must be free to rotate. We turn now to multidimensional constrained gradient design, which is the primary problem addressed in this work.

We now define the solution space consisting of three separate discrete-time waveforms along each axis, $G_x[n]$, $G_y[n]$, and $G_z[n]$, which must collectively satisfy the quadratic constraints of Eqs. [3] and [4]. The boundary constraints and moment constraints (Eqs. [5] and [6]) are applied separately for each of the dimensions. Overall, the problem is now quadratically constrained. In this work we address both linear and quadratic solution methods.

Summary of Constraints

Before we formulate the solutions to the gradient design problem, it is useful to summarize the constraints for discrete-time waveform design. Table 1 lists the four types of constraint for gradient design problems, and the number of instances of each in gradient design. The quadratic inequality constraints are the prime source of complexity in gradient design.

Convex-Optimization Methods

A particular class of constrained optimization problems, known as convex-optimization problems, have been studied extensively. For many types of convex-optimization problems, very efficient and robust solution methods have been developed. These methods are guaranteed to find the globally-optimum solution, if a solution exists. In the following sections, we describe different ways to express the gradient design constraints as standard convex-optimization problems so that they can be solved efficiently and reliably. Table 2 summarizes the number of variables and constraints of each of the methods that is discussed in the following sections.

Table 1
Basic Design Constraints for Freely-Rotatable Gradient Waveform Design, Including the Type of Constraint and the Number of Constraints in the Design of a *D*-Dimensional, *N*-Point Waveform with *Q* Moments Constrained

Constraint	Type	Number
Current (gradient amplitude)	Quadratic inequality	*N*
Voltage (gradient slew rate)	Qudaratic inequality	*N*
Gradient moments	Linear equality	$D \times Q$
Boundary values	Linear equality	2*D*

Table 2
Approximate Number (Assuming Large *N*) of Variables and Constraints for Simple-LP, L1-Norm and SOCP Formulations of Gradient Design*

Formulation	Number of variables	Number of constraints
Simple LP	*ND*	$2^{D+1}NP$
L1-norm	3*ND*	$2N(P + 2D)$
SOCP	*ND*	2*N*

*N is the number of time points, D is the number of dimensions, and P is the number of piece-wise linear constraints with non-negative coefficients.

Conversion to Linear Inequality Constraints

Both absolute-value and equality constraints can be equivalently expressed as two inequality constraints. A single absolute-value constraint $a|x| \leq b$ can be replaced by two linear constraints, $ax \leq b$ and $-ax \leq b$. An equality constraint of the form $ax = b$ can be replaced by the two inequalities $ax \leq b+\epsilon$ and $-ax \leq -b + \epsilon$. This is desirable in practical optimization, as it allows the tolerance ϵ to be different for different constraints.

Using this formulation, the constraints of Eqs. [1], [2], [5], and [6], as well as the boundary constraints can all be expressed as linear inequality constraints on the discrete-time gradient waveform.

Quadratic Constraints Expressed as Linear Constraints

Many linear programming (LP) algorithms require constraints to be expressed as a linear equality or inequality in the variables. Each quadratic constraint may be approximated by multiple linear constraints, as has been used for complex filter design (17). This is done in 2D, for example, by approximating the circle $G_x^2[n] + G_y^2[n] = G_{max}^2$ as a series of P lines defined by

$$\cos(\theta_p)G_x[n] + \sin(\theta_p)G_y[n] \leq G_{max}\cos\left(\frac{\pi}{P}\right) \quad \forall p = 1 \ldots P \qquad [8]$$

where $\theta_p = 2\pi\frac{p-0.5}{P}$. Figure 3 shows this piecewise linear approximation to a 2D quadratic constraint with $P = 8$. For all of the 2D examples in this work, we use $P = 16$.

For 3D quadratically constrained problems, it is possible to perform a piecewise-linear approximation to a sphere. A simple way to do this is to consider the surface of the sphere $|\vec{r}| = c$ in the first octant where the components of $\vec{r}$ are all positive (Fig. 4). By placing points on the surface of the sphere, triangles with roughly equal area are constructed, and the constraints can be expressed in the form

$$\vec{n} \cdot \vec{r} \leq \vec{n} \cdot \vec{V} \qquad [9]$$

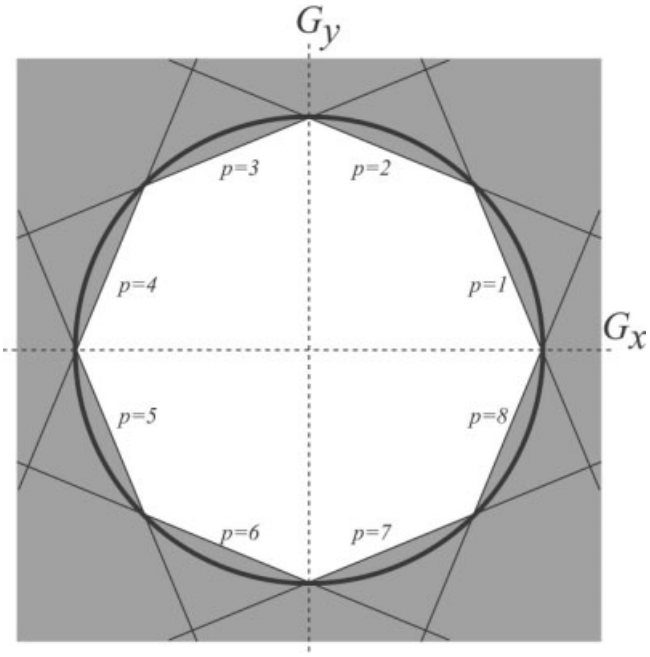

FIG. 3. Piecewise linear approximation to quadratic constraints, as defined by Eq. [8] with $P = 8$. The white area represents the allowable values of the 2D amplitude. Piecewise linear limits can similarly be applied to either the voltage or the slew rate.

where $\vec{n}$ is a vector normal to the triangle, i.e., $\vec{n} = (\vec{B} - \vec{A}) \times (\vec{C} - \vec{A})$, and $\vec{V}$ is the position vector of any of the triangle corners, ($\vec{A}$, $\vec{B}$, or $\vec{C}$).

For the 3D examples in this work, we subdivide the first quadrant into nine planes using the points shown in Fig. 4. The entire sphere can then be represented by the 72 planes generated with all permutations of positive and negative signs in the individual $\vec{n}$ vectors.

Simple-LP Formulation

The problem, with only linear inequality constraints, can be solved using LP. The "standard LP" form of a problem is to find the column vector $\boldsymbol{x}$ that minimizes a cost function $\boldsymbol{f}^T\boldsymbol{x}$ subject to the constraints $\boldsymbol{Ax} \leq \boldsymbol{b}$. (In all cases, the inequality is applied to *each* row of the column vectors.) The matrix $\boldsymbol{A}$ and column vector $\boldsymbol{b}$ are formed by combining all of the linear constraint equations for amplifier and pulse sequence constraints. We will refer to this formulation of the problem as the "simple-LP" formulation.

The cost function in the simple-LP formulation is linear in the gradient values. The minimization of such a cost function is not particularly useful. As such, the actual optimization consists of a series of feasibility tests, as described below. For the simple-LP formulation, we simply choose $\boldsymbol{f}$ to be a column vector of ones.

The LP formulation for an N-point waveform uses ND variables with roughly $2^{D+1}NP$ constraints, where D is the number of dimensions and P is the number of piecewise linear constraints on the gradient amplitude and voltage amplitude for which coefficients are all positive (i.e., the number of constraints in the first quadrant or octant). Appendix A shows the complete simple-LP formulation for a 2D freely-rotatable gradient design problem.

L1-Norm Formulation

An alternative to the simple-LP formulation is the L1-norm formulation, which alters the number of constraints and can produce different solutions to the problem (18).

The L1-norm formulation uses standard LP to minimize the L1-norm (absolute value) of the gradient and slew voltage by adding "slack variables" to the optimization problem (19). In addition to solving for $G_x[n]$, we solve a set of variables $H_x[n]$, that converge to $|G_x[n]|$, and a set of variables $S_x[n]$ that converge to $|\alpha G_x[n] + \beta G_x[n+1]|$.

The slack variables are forced to converge by first adding the following linear gradient constraints to the problem:

$$\begin{aligned} -H_x[n] + G_x[n] &\leq 0 \\ -H_x[n] - G_x[n] &\leq 0 \end{aligned} \qquad [10]$$

Additionally, we add the following slew-rate constraints:

$$\begin{aligned} -S_x[n] + \alpha G_x[n] + \beta G_x[n+1] &\leq 0 \\ -S_x[n] - \alpha G_x[n] - \beta G_x[n+1] &\leq 0 \end{aligned} \qquad [11]$$

These constraints will force the $H_x[n]$ and $S_x[n]$ variables to approach the appropriate absolute value when combined with minimization of the following cost function:

$$J(S_x[n], H_x[n]) = \sum_{n=1}^{N} (H_x[n] + S_x[n]) \qquad [12]$$

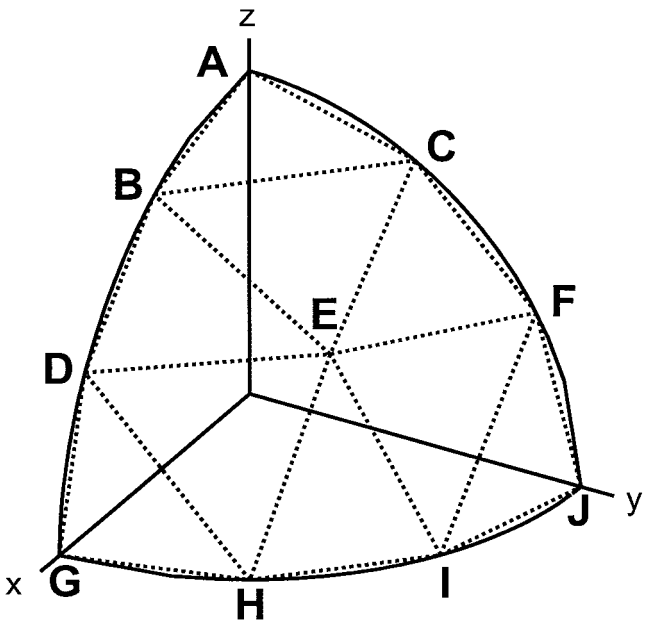

FIG. 4. Piecewise linear approximation to the spherical surface representing 3D quadratic constraints. The points shown are permutations of $\langle 1, 0, 0\rangle$, $\langle \frac{\sqrt{3}}{2}, \frac{1}{2}, 0\rangle$, and $\langle \frac{1}{\sqrt{3}}, \frac{1}{\sqrt{3}}, \frac{1}{\sqrt{3}}\rangle$.

For 2D and 3D problems, an appropriate set of variables $H_y[n]$, $S_y[n]$, $H_z[n]$ and $S_z[n]$ would be added. Constraints for these variables are expressed as in Eqs. [10] and [11], and the variables would be added to the cost function in Eq. [12].

The simple-LP cost function of all ones simply tries to make individual gradient axes closer to their negative amplitude limits. However, the L1-norm cost function is physically meaningful, as it tends to minimize the magnitude of both gradient current and voltage, which will improve the heating characteristics of the waveform.

When the L1-norm formulation is used, the piecewise linear constraints on gradient amplitude may be reduced by replacing the constraint on $G_x[n]$, $G_y[n]$, and $G_z[n]$ with equivalent constraints on $H_x[n]$, $H_y[n]$, and $H_z[n]$. Similarly, the voltage constraints may be replaced with constraints on $S_x[n]$, $S_y[n]$, and $S_z[n]$. Since all of the slack variables are constrained to be non-negative, only the gradient amplitude and voltage-limit constraints with positive coefficients are needed. This reduces the number of gradient amplitude constraints by a factor of 2^D, where D is the number of gradient axes, and is the primary advantage of the L1-norm formulation compared to the simple-LP formulation.

The L1-norm formulation uses $3ND$ variables, and approximately $2N(P + 2D)$ constraints. For 2D or 3D problems, the number of constraints is often much smaller than that of the simple-LP formulation. Additionally, as described by Xu et al. (18), L1-norm programming tends to find solutions where some or many of the variables are zero. This may be advantageous in gradient design, as solutions with a lower gradient or slew duty cycle result in lower gradient heating.

Second-Order Cone Programming (SOCP) Formulation

SOCP (20) is a method that finds the solution $\boldsymbol{x}$ that minimizes a linear cost function $\boldsymbol{f}^T\boldsymbol{x}$ subject to the SOC constraints

$$\|\boldsymbol{A}\boldsymbol{x} + \boldsymbol{b}\|_2 \leq \boldsymbol{C}\boldsymbol{x} + \boldsymbol{d}. \qquad [13]$$

First, we note that this constraint is a superset of the linear constraints in LP. Second, the cost function is linear, as with the simple-LP formulation described above, and is chosen in the same manner (as all ones).

The SOCP formulation of the gradient design problem begins with Eqs. [5] and [6].

Although these constraints could be reduced by a factor of 2^D compared to the simple-LP or L1-norm formulations, this has little effect on convergence time. The main advantage of the SOCP formulation is that the quadratic limits of Eqs. [3] and [4] result in a total of $2N$-1 constraints, regardless of the number of gradient dimensions. Additionally, the SOCP formulation does not approximate the quadratic gradient limits, which sometimes results in slightly shorter-duration solutions. Lobo et al. (20) have generously made the SOCP software available in the form of C routines and a Matlab interface at http: //www.stanford.edu/~boyd/group_index.html.

Reduction of Constraints

Because the time to find a solution increases with the number of constraints, it is useful to try to further reduce the number of constraints. Assuming that the slew-rate constraints are met, there will be gradient amplitude constraints near the end points that are redundant. Specifically, if the (minimum) distance from the start or end gradient to a linear or quadratic gradient constraint is ΔG, then that constraint is redundant for at least a time $\frac{L\Delta G}{\eta V_{max} + RG_{max}}$.

Minimum-Time Solutions

The minimum-time gradient design problem is to find N_{min}, the minimum value of N for which a solution exists. LP functions can be called sequentially with different values of N. We first assume that either $\tilde{G}(0) = 0$ or $\tilde{G}(n\tau) = 0$. If a solution exists for N, then $N_{min} \leq N$. Otherwise, $N_{min} \geq N$.

This suggests the use of a binary-search or "bisection" technique, which divides the unknown interval containing N_{min} on each call. We begin with estimates of the upper and lower bounds N_u and N_l on N. First, these are tested to ensure that they are in fact upper and lower bounds. If they are not, both bounds are raised or lowered accordingly and retested. Once N_u and N_l have been verified, we set N as close as possible to $N_l + \nu(N_u - N_l)$. Depending on whether or not a solution exists, either N_u or N_l is set to N, and the process is repeated. We have empirically determined $\nu = 0.8$, because an existing solution is found considerably more quickly than the lack of a solution using both SOCP and Matlab's *linprog()* function.

VALIDATION

We implemented the above formulation using Matlab 6.0 with functions from the Mathworks Optimization toolbox (Mathworks, Natick, MA). Specifically, we use the *linprog()* function, as well as the *socp()* function described above. Our Matlab functions are available for general use, as described briefly in Appendix B.

We begin by comparing the time required to solve the minimum time gradient-area-nulling problem using the simple-LP, L1-norm, and SOCP methods. All tests used Matlab 6.0 on 1.8 GHz Athlon PCs running Linux. The bisection formulation was identical for all three methods, and the comparison was performed for 1D, 2D, and 3D problems.

We generated 1000 different starting conditions for the given dimension with boundary values within the magnitude constraint for the given solution method. A sample period of $\tau = 20$ μs was used, which assumes a gradient amplifier bandwidth of <25 kHz. The gradient and zeroth moment of the gradient were then rewound to zero using the bisection method described above. Each step of the bisection method was solved using a simple-LP, L1-norm, or SOCP formulation. The times required to solve the rewinder problem for each waveform and each formulation method were recorded. In all cases we used a maximum gradient amplitude of 40 mT/m, and a constant-slew-rate model with 150 T/m/s maximum slew rate. For 2D and 3D, the rewinders are limited by the quadratic constraints described above.

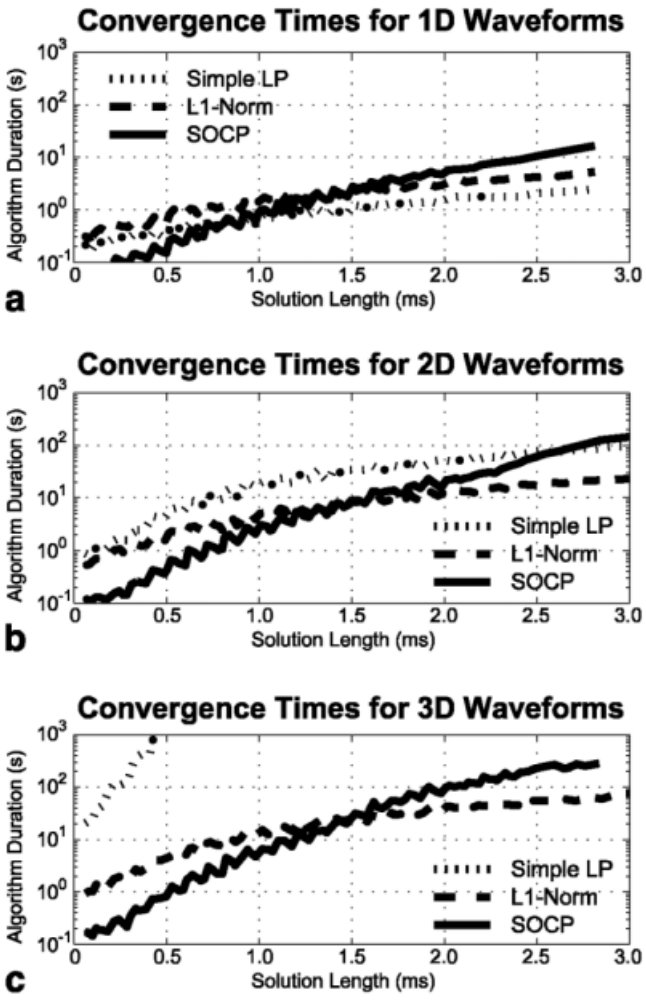

FIG. 5. Convergence time for 1D (**a**), 2D (**b**), and 3D (**c**) time-optimal gradient design using simple-LP (dotted line), L1-norm (dashed line), and SOCP (solid line) formulations. Although the simple-LP formulation is the most efficient for 1D design problems, the L1-norm is significantly better for 2D and 3D problems. SOCP outperforms L1-norm in 2D and 3D problems, except when the solution length turns out to be very long.

Figure 5 compares convergence times for the three methods for 1D, 2D, and 3D design problems. In all cases, the solution length is almost identical for simple-LP, L1-norm, and SOCP, although SOCP sometimes gives a very slightly shorter solution due to greater usage of the gradient amplitude or slew rate. Not surprisingly, convergence time increases with the solution length. SOCP formulation is fastest regardless of dimension for most practical waveforms (i.e., duration < 1 ms), and is significantly faster than the other methods as the number of gradient dimensions increases to 2 or 3.

EXAMPLES

Here we present several examples showing applications of LP for time-optimal gradient design. We begin with 1D examples illustrating that LP produces the time-optimal waveforms. Next we show 2D examples, particularly for use in spiral imaging. Finally, we show 3D examples for double-oblique or oblique spiral scans. All of our examples use the L1-norm formulation.

Moment-Nulled Waveforms

For a constant-amplitude-limit, constant-slew-rate-limit gradient, the minimum time waveforms to produce a given zeroth, first and/or second moment are generally triangular or trapezoidal waveforms. However, calculation of the segments sometimes must be solved numerically.

Our first example is the generation of a simple 1D moment-nulled phase-encoding gradient. The boundary constraints on the pulse waveform are $G_x[0] = G_x[N] = 0$, and the desired k-space area and first moments are $\Delta\vec{k} = \vec{K}_{des}$ and $m_1 = 0$. In our example, we set $k_{des} = 0.40$ mm^{-1}, $G_{max} = 40$ mT/m, and maximum gradient slew rate $\frac{\psi}{L} = 150$ T/m/s.

The resulting gradient waveform, k-space trajectory, slew rate, and first moment are shown in Fig. 6. The gradient is a bipolar combination of a trapezoidal lobe with a triangular lobe, as can reasonably be expected given the amplitude- and slew-limited constraints in one dimension. Note that either the gradient amplitude limit or the slew-rate limit is always met, which should be the case for a minimum-time preparatory gradient in one dimension.

Echo-Planar Transition Gradients

The second example shows the design of a minimum-time waveform that transitions between successive lines of an echo-planar imaging (EPI) trajectory, as described by Dale and Duerk (9). For consistency, we use the same gradient and slew limits as in Ref. 9 (20 mT/m and 200 T/m/s, respectively), with the assumption that the gradients can be freely rotated to any oblique in-plane position. The EPI trajectory uses a 20 mT/m readout gradient, with an 0.8-cm^{-1} phase-encode area between lines. In our formulation, we specify $G_x[1] = -G_x[N] = 20$ mT/m, $G_y[1] = G_y[N] = 0$ mT/m, $\Delta k_x = 0$ mm^{-1}, $\Delta k_y = 0.08$ mm^{-1}, and $\tau = 1$ μs.

The result, which is shown in Fig. 7, has a total duration of 245 μs, as compared to 243 μs in Ref. 9. The solutions with both methods look very similar, and the minor difference between them is most likely due to the way the end-point constraint is formulated. Interestingly, this gradient is not zero at either end point. However, because of the symmetry of the problem, the bisection method of finding the minimum-time gradient still works.

Time-Optimal Radial Rewinders

A minimum gradient waveform design in one dimension can generally be solved exactly and analytically. However, a 2D design is not so simple. Here we consider spiral imaging, where interleaved spiral waveforms are played by rotating the waveform in the x-y gradient plane. For the trajectory to be played at arbitrary rotation angles, the gradient and slew rate *vector* magnitudes must be within slew-rate constraints.

Spiral waveform design methods have been addressed previously (15,21–23). The spiral waveform can be re-

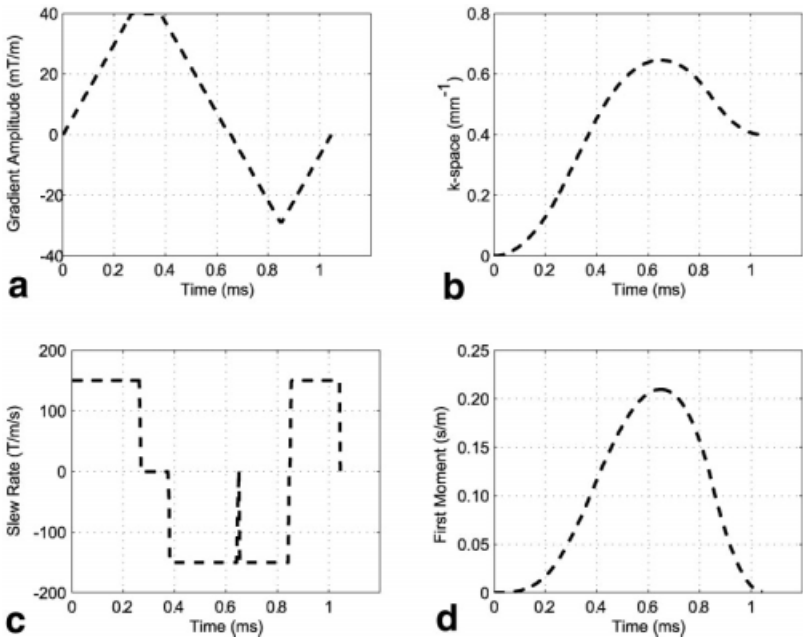

FIG. 6. (**a**) First-moment-nulled gradient waveform, (**b**) corresponding *k*-space trajectory, (**c**) gradient slew rate, and (**d**) gradient first moment, all plotted as functions of time for example A. The gradient waveform has a duration of 1.048 ms.

wound by separately rewinding each axis with both amplitude (current) and voltage limits set to $1/\sqrt{2}$ times the individual axis limits. This is adequate for applications in which the spiral readout duration is long but is not time-optimal. In cases such as spiral SSFP (24) or reversed-spiral (25) imaging, it is desirable to rewind or null the first moment of the gradient as well. In this example, we designed a time-optimal rewinder for spiral gradient waveforms, as well as a rewinder for a first-moment-nulled spiral waveform.

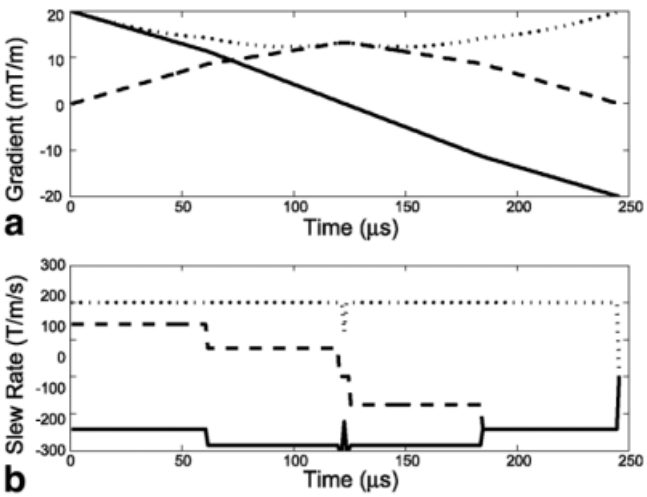

FIG. 7. Gradient waveforms (**a**) and slew rates (**b**) for an echo-planar readout/phase-encode transition. Gradients and slew rates are shown for the *x*-axis (solid line), *y*-axis (dashed line), and magnitude (dotted line). Our method performs as well as the time-optimal method described in Ref. 9. The apparent glitch in the slew rate at the center of the plot occurs because the L1-norm formulation attempts to minimize the magnitude of the slew rate. The symmetry of the problem means that any small dead time in the gradient occurs at the center. With a finer sampling rate, this glitch would likely disappear.

For this example, we used a spiral waveform similar to that used for SSFP imaging (24,26). The design assumes 60 spiral interleaves to achieve a resolution of 1.25 mm and an FOV of 20 cm with a readout duration of 1.7 ms.

The optimization goal is to rewind the gradient waveforms and zeroth moment vector simultaneously to zero as quickly as possible. The rewinder gradient vector initially equals the final gradient of the readout, and ends at zero in both dimensions. Combined with the constraint of rewinding the zeroth moment vector, this gives six equality constraints. Figure 8 shows the spiral gradient waveform and rewinder characteristics. All quantities reach zero at the end of the waveform, except the first moment. As with the 1D example, either the gradient magnitude or slew-rate magnitude limit is reached for the entire duration of the rewinder.

The spiral rewind problem can be repeated for the case in which the first moments are also rewound at the end of the waveform. This adds a constraint in each axis, for a total of eight equality constraints. The L1-norm solution is shown in Fig. 9. For nulling of the first moments, the minimum-time waveform is significantly increased from 0.66 ms to 1.23 ms. If the two axes were rewound separately (as is commonly performed), each using 70% of the maximum power, the duration would be closer to 1.8 ms. In rapid imaging sequences such as SSFP, 0.4 ms is a significant time reduction (i.e. 10% of the TR or 25% of the data acquisition time).

Double-Oblique 3D Gradient Design

In certain cases, such as double-oblique scans or oblique-plane 3D spiral scans, the gradient vector must be rotated freely in three dimensions. The 3D example we show here

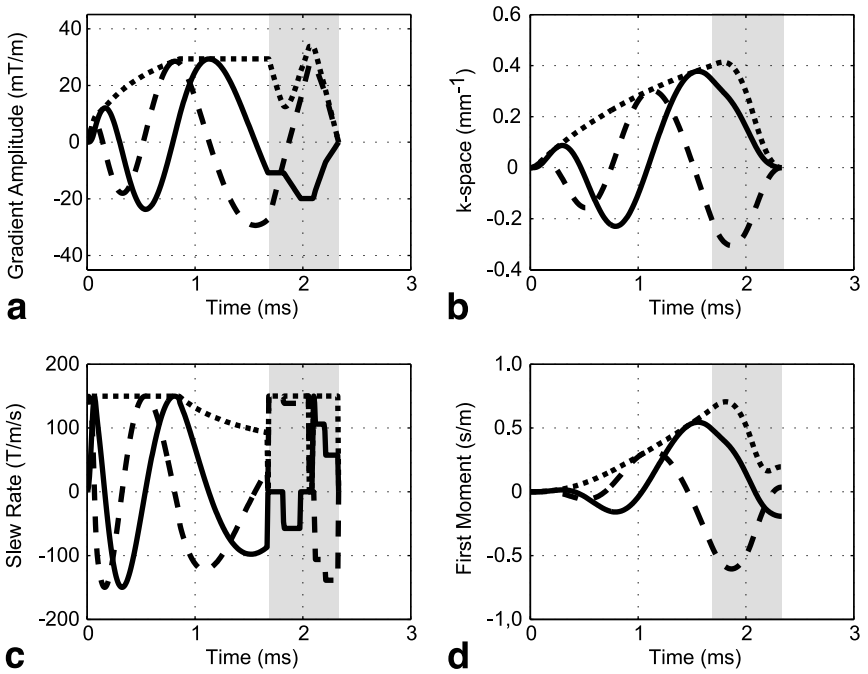

FIG. 8. Gradient waveforms (**a**), *k*-space trajectory (**b**), slew rates (**c**), and first moment (**d**) for a simple rewinder waveform (gray region) for a 2D-spiral imaging gradient. Each plot shows *x* (solid line) and *y* (dashed line) components, as well as the magnitude (dotted line). The *k*-space-only rewinder lasts for 0.66 ms, and has a significant residual first moment.

pertains to the latter, where spiral scanning is combined with phase-encoding in the *z*-axis (27). All gradients are rewound at the end of the sequence. To minimize the overall time, the *z*-axis rewinder is played out simultaneously with the spiral rewinder.

The problem is formulated the same way as used for the simple spiral-rewinder in example B, except that now a phase-encode gradient is included before the spiral readout. The 3D rewinder brings the net area of all three gradient axes to zero. The minimum-time solution is shown in Fig. 10.

General Oblique Cartesian Cases

Another area where convex-optimization solutions can be very useful is general oblique Cartesian scanning. For oblique spin-warp or EPI scans, one usually calculates the gradient lobes by first examining how many gradient axes are on simultaneously at a given point in the sequence. Maximum limits are used for each point in the sequence, as described by Bernstein et al. (28). Although this approach is simple and effective, in certain cases it overconstrains the gradient de-

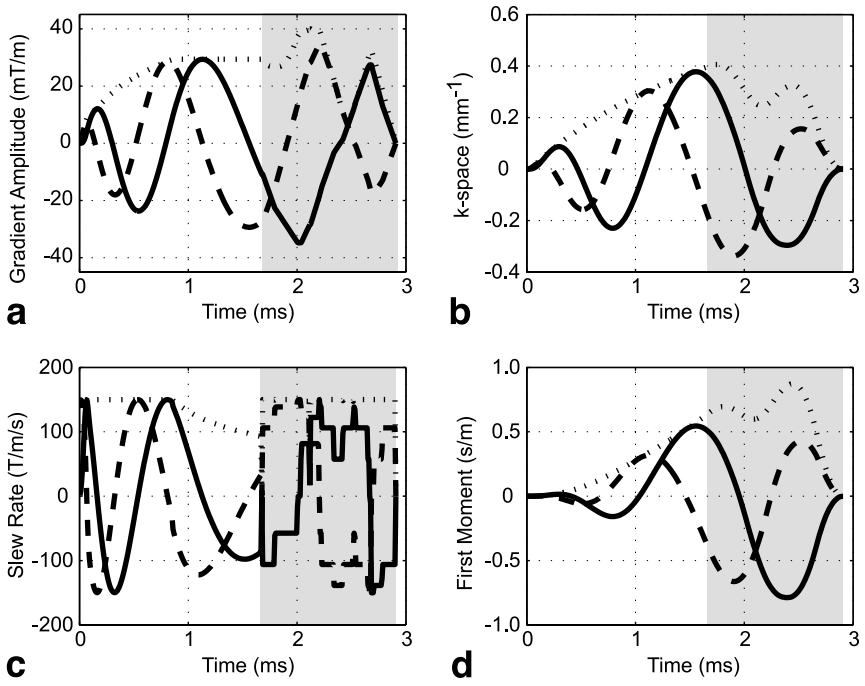

FIG. 9. Gradient waveforms (**a**), *k*-space trajectory (**b**), slew rates (**c**), and first moment (**d**) for an m_1-nulled rewinder waveform (gray region) for a 2D-spiral imaging gradient. Each plot shows *x* (solid line) and *y* (dashed line) components, as well as the magnitude (dotted line). The m_1-nulled rewinder lasts for 1.23 ms, and rewinds the gradient, *k*-space location, and the first moment.

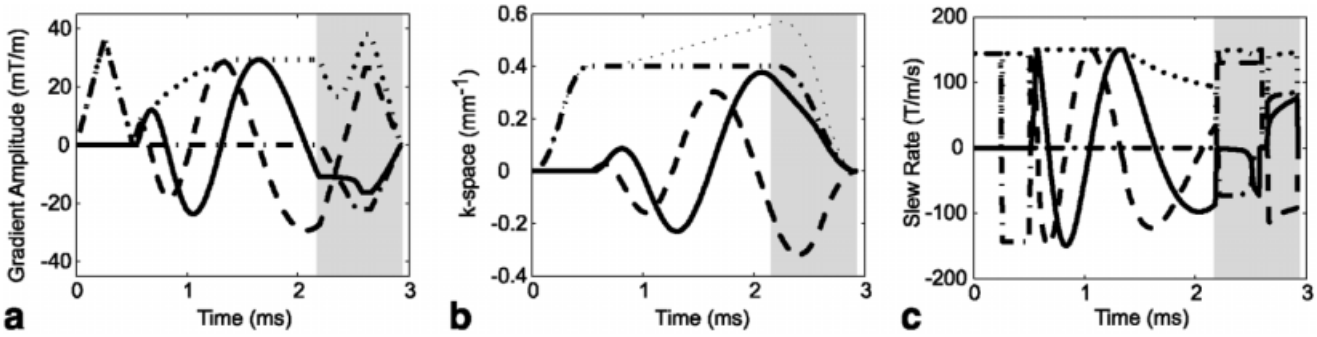

FIG. 10. Gradient waveforms (**a**), *k*-space trajectory (**b**), and slew rates (**c**) for a 3D rewinder waveform (gray region) for a "stack-of-spirals" imaging gradient. Each plot shows *x* (solid line), *y* (dashed line), and *z* (dash-dot line) components, as well as the magnitude (dotted line). The rewinder gradient lasts for 0.74 ms.

sign. When more than one gradient is on, this method reduces the available gradient power, as shown in Fig. 11.

Using the simple-LP formulation, the gradient amplitude and slew-rate constraints for any oblique angle can be expressed as linear constraints. For example, for 2D oblique scans at an oblique angle, ϕ, the limits are

$$G_x[n]\cos(\phi + \Delta\phi) + G_y[n]\sin(\phi + \Delta\phi) \leq G_{max} \quad [14]$$

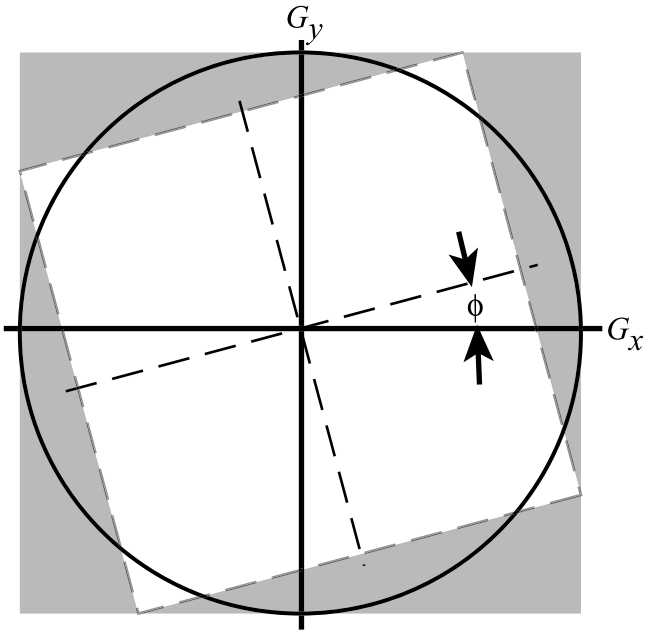

FIG. 11. Gradient amplitude usage for different oblique-scan strategies. The dark gray square represents all usable gradient amplitude, and the circle represents the quadratically-constrained amplitude if the gradient is designed to be freely rotatable. If gradients are designed completely independently, then the amplitude limits on each axis must be reduced so that the worst-case gradient still lies within the dark gray square. This reduces usage of the gradient amplitude (as shown by the white area and dashed lines) for a rotation angle of f = ϕ. With constraints tailored to the specific oblique angle, all gradient power is available for any rotation angle.

and

$$(\alpha G_x[n] + \beta G_x[n+1])\cos(\phi + \Delta\phi) + (\alpha G_y[n] + \beta G_y[n+1])\sin(\phi + \Delta\phi) \leq \psi \quad [15]$$

where $\Delta\phi$ takes on values $-\pi/2$, 0, $\pi/2$, and π; and α, β, and ψ are defined by Eq. [7]. Similar linear constraints could also be applied for 3D scans. Compared with previous techniques (28), this technique will ensure that all gradient power is always available.

As an example, we consider the echo-planar transition of example B, where the oblique scan plane is rotated by 30° from the physical gradient axes. Figure 12 shows the resulting waveforms, which are faster than that shown in Fig. 7, as more gradient power is available for both the amplitude and the slew rate. The off-axis case results in a

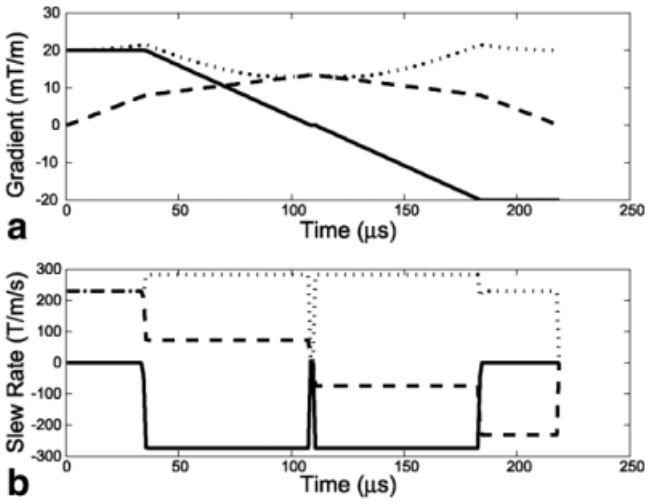

FIG. 12. Gradient waveforms (**a**) and slew rates (**b**) for the echo-planar transition of example B, but with gradients optimized for the case in which logical and physical gradients are separated by 30°C. For this example, the waveform is slower than the on-axis case. However, it is still faster than that in example B. Gradients and slew rates are shown for the *x*-axis (solid line), *y*-axis (dashed line), and magnitude (dotted line).

longer waveform, because slewing in two logical axes must be performed by one physical axis.

DISCUSSION

The design of many minimum-time gradient waveforms can be expressed as a constrained optimization problem. With some manipulation, the problem can be posed as a standard-LP problem, for which many efficient solving methods have been developed. The formulation described solves minimum-time gradient problems wherein the initial and final gradient values, and the desired moments are specified, and the gradient either starts or ends at zero.

Time-Optimality

Whether or not one can prove time-optimality is an interesting question. For 1D cases, this can be done, and our results indicate the current algorithm produces the minimum-time solution. For more complex cases for which there is no analytic solution, it is not possible to prove the time-optimality of the solution. Based on the principles of convex-optimization techniques, we assume that the solutions are time-optimal. Additionally, the simple-LP and L1-norm formulations always give the same duration gradient.

Formulation Options

The minimum-time gradient problem, as expressed above, is a series of feasibility problems that use solution vectors of different lengths. We have shown three different problem formulations. First, the problem can be solved simply as a standard-LP problem, using $G_x[n]$, $G_y[n]$, and $G_z[n]$ variables, representing the gradient on each axis. Second, the L1-norm formulation adds additional slack variables, $H_x[n]$, $H_y[n]$, and $H_z[n]$, representing the gradient magnitudes and $S_x[n]$, $S_y[n]$, and $S_z[n]$ representing the voltage magnitude to further reduce the number of constraints. Third, the SOCP formulation uses $G_x[n]$, $G_y[n]$, and $G_z[n]$ variables and quadratic constraints on both gradient amplitude and gradient voltage.

All three formulation methods use a cost function that is linear in the variables. In the L1-norm formulation, the cost function minimizes some linear combination of the absolute values of variables. However, it is important to note that this work describes *minimum-time* waveform design. In all formulations, the time optimization is done using feasibility tests. Thus the cost functions do not necessarily have a physical meaning.

Depending on the uniqueness of the minimum-time solution for a set of constraints and sample rate, the cost function may or may not affect the resulting solution. In previous work by Simonetti et al. (7,8), for example, a cost function was chosen to minimize the power dissipated in the gradient coils. Such a quadratic cost function could be expressed if the SOCP formulation were used. Then, by allowing the solution to be longer than the minimum-time solution, the waveform duration could be traded for reduction of the cost function. Depending on the formulation, similar trade-offs could be made between time and other cost functions that might minimize, for example, eddy-current effects (7,8).

In terms of convergence times, the simple-LP formulation is advantageous compared to the L1-norm only for 1D problems. For 2D or 3D problems for which the solutions consist of $\leq$75 time samples (1.5 ms with ΔT = 20 μs), the SOCP formulation is the fastest formulation. Given that the SOCP formulation also uses the available gradient limits slightly more efficiently than either the simple-LP or the L1-norm formulation, it is clearly the best option. However, if SOCP software is not available, the L1-norm formulation also performs very well for 2D or 3D problems.

The discretely-sampled waveforms $G_x[n]$, $G_y[n]$, and $G_z[n]$ were chosen for simplicity. The sampling interval was chosen to be small enough to fully utilize gradient fidelity, as well as to accurately approximate integrals using discrete sums. We assume that the slew-rate or voltage limit will result in waveforms that do not exceed the gradient system bandwidth. Although this is usually true, there may be exceptions that make it desirable to band-limit the waveforms in the design process. This could be achieved by expressing the gradient waveforms as a linear combination of a band-limited basis set, such as a set of band-limited sinc-like functions, or a limited Fourier basis set. Such a reformulation might reduce the number of variables in the optimization, resulting in reduced convergence time.

CONCLUSIONS

Minimum-time, multidimensional gradient designs are an increasingly important part of MRI sequences. We have shown a method that can deliver time-optimal gradients given a variety of constraints, including amplitude, slew rate, end points, and gradient moments. Our method uses standard LP tools, which are sufficiently robust and efficient to reliably solve problems that currently have no analytical solution.

APPENDIX A

Simple-LP Gradient Design Formulation

To actually solve the gradient design problem using LP or SOCP, the matrix $\boldsymbol{A}$ and vector $\boldsymbol{b}$ are constructed using all of the constraints discussed in the text. For the simple-LP formulation, the constraint matrix form is as follows:
Horizontal lines separate four different types of constraints: boundary, current, voltage, and area. Here $C_p = \cos(\theta_p)$ and $S_p = \sin(\theta_p)$, with θ_p defined as in Eq. [8]. Also, $G'_{max} = G_{max}\cos(\frac{\pi}{P})$ and $\psi' = \psi\cos(\frac{\pi}{P})$. In the above expression, ϵ can have different values for different constraints. (As described in the text, γ is the gyromagnetic ratio, τ is the sampling period, and ψ is defined in Eq. [7]).

$$\begin{pmatrix}
1 & 0 & \cdots & 0 & 0 & 0 & 0 & \cdots & 0 & 0 \\
-1 & 0 & \cdots & 0 & 0 & 0 & 0 & \cdots & 0 & 0 \\
0 & 0 & \cdots & 0 & 0 & 1 & 0 & \cdots & 0 & 0 \\
0 & 0 & \cdots & 0 & 0 & -1 & 0 & \cdots & 0 & 0 \\
0 & 0 & \cdots & 0 & 1 & 0 & 0 & \cdots & 0 & 0 \\
0 & 0 & \cdots & 0 & -1 & 0 & 0 & \cdots & 0 & 0 \\
0 & 0 & \cdots & 0 & 0 & 0 & 0 & \cdots & 0 & 1 \\
0 & 0 & \cdots & 0 & 0 & 0 & 0 & \cdots & 0 & -1 \\
\hline
C_1 & 0 & \cdots & 0 & 0 & S_1 & 0 & \cdots & 0 & 0 \\
\vdots & \vdots & \ddots & \vdots & \vdots & \vdots & \vdots & \ddots & \vdots & \vdots \\
C_P & 0 & \cdots & 0 & 0 & S_P & 0 & \cdots & 0 & 0 \\
0 & C_1 & \cdots & 0 & 0 & 0 & S_1 & \cdots & 0 & 0 \\
\vdots & \vdots & \ddots & \vdots & \vdots & \vdots & \vdots & \ddots & \vdots & \vdots \\
0 & C_P & \cdots & 0 & 0 & 0 & S_P & \cdots & 0 & 0 \\
\vdots & \vdots & \ddots & \vdots & \vdots & \vdots & \vdots & \ddots & \vdots & \vdots \\
0 & 0 & \cdots & 0 & C_1 & 0 & 0 & \cdots & 0 & S_1 \\
\vdots & \vdots & \ddots & \vdots & \vdots & \vdots & \vdots & \ddots & \vdots & \vdots \\
0 & 0 & \cdots & 0 & C_P & 0 & 0 & \cdots & 0 & S_P \\
\hline
\alpha C_1 & \beta S_1 & \cdots & 0 & 0 & \alpha S_1 & \beta S_1 & \cdots & 0 & 0 \\
\vdots & \vdots & \ddots & \vdots & \vdots & \vdots & \vdots & \ddots & \vdots & \vdots \\
\alpha C_P & \beta C_P & \cdots & 0 & 0 & \alpha S_P & \beta S_P & \cdots & 0 & 0 \\
\vdots & \vdots & \ddots & \vdots & \vdots & \vdots & \vdots & \ddots & \vdots & \vdots \\
0 & 0 & \cdots & \alpha C_1 & \beta C_1 & 0 & 0 & \cdots & \alpha S_1 & \beta S_1 \\
\vdots & \vdots & & \vdots & \vdots & \vdots & \vdots & & \vdots & \vdots \\
0 & 0 & \cdots & \alpha C_P & \beta C_P & 0 & 0 & \cdots & \alpha S_P & \beta S_P \\
\hline
\frac{\gamma}{2\pi}\tau & \frac{\gamma}{2\pi}\tau & \cdots & \frac{\gamma}{2\pi}\tau & \frac{\gamma}{2\pi}\tau & 0 & 0 & \cdots & 0 & 0 \\
-\frac{\gamma}{2\pi}\tau & -\frac{\gamma}{2\pi}\tau & \cdots & -\frac{\gamma}{2\pi}\tau & -\frac{\gamma}{2\pi}\tau & 0 & 0 & \cdots & 0 & 0 \\
0 & 0 & \cdots & 0 & 0 & \frac{\gamma}{2\pi}\tau & \frac{\gamma}{2\pi}\tau & \cdots & \frac{\gamma}{2\pi}\tau & \frac{\gamma}{2\pi}\tau \\
0 & 0 & \cdots & 0 & 0 & -\frac{\gamma}{2\pi}\tau & -\frac{\gamma}{2\pi}\tau & \cdots & -\frac{\gamma}{2\pi}\tau & -\frac{\gamma}{2\pi}\tau
\end{pmatrix}
\begin{pmatrix}
G_x[1] \\ G_x[2] \\ \vdots \\ G_x[N-1] \\ G_x[N] \\ G_y[1] \\ G_y[2] \\ \vdots \\ G_y[N-1] \\ G_y[N]
\end{pmatrix}
\leq
\begin{pmatrix}
\epsilon \\ \epsilon \\ \epsilon \\ \epsilon \\ \epsilon \\ \epsilon \\ \epsilon \\ \epsilon \\
\hline
G'_{max} \\ \vdots \\ G'_{max} \\ G'_{max} \\ \vdots \\ G'_{max} \\ \vdots \\ \vdots \\ G'_{max} \\ \vdots \\ G'_{max} \\
\hline
\psi' \\ \vdots \\ \psi' \\ \vdots \\ \vdots \\ \psi' \\ \vdots \\ \psi' \\
\hline
\Delta k_x + \epsilon \\ -\Delta k_x + \epsilon \\ \Delta k_y + \epsilon \\ -\Delta k_y + \epsilon
\end{pmatrix} \quad [16]$$

APPENDIX B

Matlab Software

The general Matlab functions used in the examples are available at http: //www-mrsrl.stanford.edu/ brian/mintgrad/. The basic functions are as follows:

1. mintimegrad(): Repeatedly calls either *lpgrad()* or *socpgrad()* to find the minimum-time solution to a set of multidimensional gradient design constraints.
2. socp(): Solves an SOCP problem. This is available via http: //www.stanford.edu/~boyd/group_index.html.
3. lpgrad(): Formulates a problem as simple-LP or L1-norm, and uses *linprog()* to find a solution.
4. socpgrad(): Formulates a problem using the SOCP formulation, and uses *socp()* to find a solution.

REFERENCES

1. Zur Y, Stokar S, Bendel P. An analysis of fast imaging sequences with steady-state transverse magnetization refocusing. Magn Reson Med 1988;6:175–193.
2. Hennig J, Nauerth A, Friedburg H. RARE imaging: a fast imaging method for clinical MR. Magn Reson Med 1986;3:823–833.
3. Oppelt A, Graumann R, Barfuss H, Fischer H, Hartl W, Shajor W. FISP—a new fast MRI sequence. Electromedica 1986;54:15–18.
4. Duerk JL, Lewin JS, Wendt M, Petersilge C. Remember true FISP? a high SNR near 1-second imaging method for T_2-like contrast in interventional MRI at .2 T. J Magn Reson Imaging 1998;8:203–208.
5. Mansfield P. Multiplanar image formation using NMR spin-echoes. J Phys Chem Solid State Phys 1977;10:L55.
6. Meyer CH, Hu BS, Nishimura DG, Macovski A. Fast spiral coronary artery imaging. Magn Reson Med 1992;28:202–213.
7. Simonetti OP, Duerk JL, Chankong V. An optimal design method for magnetic resonance imaging gradient waveforms. IEEE Trans Med Imaging 1993;12:350–360.
8. Simonetti OP, Duerk JL, Chankong V. MRI gradient waveform design by numerical optimization. Magn Reson Med 1993;29:498–504.
9. Dale BM, Duerk JL. Time-optimal control of gradients. In: Proceedings of the 10th Annual Meeting of ISMRM, Honolulu, 2002. p 2361.
10. Bolster BD, Jr, Atalar E. Minimizing dead-periods in flow-encoded or -compensated pulse sequences while imaging in oblique planes. J Magn Reson Imaging 1999;10:183–192.
11. Atalar E, McVeigh ER. Minimization of dead-periods in MRI pulse sequences for imaging oblique planes. Magn Reson Med 1994;32:773–777.
12. Pipe JG, Chenevert TL. A progressive gradient moment nulling design technique. Magn Reson Med 1991;19:175–179.
13. Heid O. The fastest circular k-space trajectories. In: Proceedings of the 10th Annual Meeting of ISMRM, Honolulu, 2002. p 2364.
14. Morgan VL, Price RR, Lorenz CH. Application of linear optimization techniques to MRI phase contrast blood flow measurements. Magn Reson Imaging 1996;14:1043–1051.
15. King KF, Foo TK, Crawford CR. Optimized gradient waveforms for spiral scanning. Magn Reson Med 1995;34:156–160.

16. Schmitt F. Gradient systems. In: Weekend Educational Course Syllabus, 10th Annual Meeting of ISMRM, Honolulu, 2002. p 477–486.
17. Chen X, Parks TW. Design of FIR filters in the complex domain. IEEE Trans ASSP 1987;35:144–153.
18. Xu H, Conolly SM, Scott GC, Macovski A. Homogeneous magnet design using linear programming. IEEE Trans Med Imaging 2000;36:476–483.
19. Gill PE, Murray W, Wright MH. Practical optimization. London: Academic Press; 1981.
20. Lobo M, Vandenberghe L, Boyd S, Lebret H. Applications of second-order cone programming. Linear Algebra Appl 1998;284:193–228.
21. Meyer CH, Pauly JM, Macovski A. A rapid, graphical method for optimal spiral gradient design. In: Proceedings of the 4th Annual Meeting of ISMRM, New York, 1996. p 392.
22. Glover GH. Simple analytic spiral *k*-space algorithm. Magn Reson Med 1999;42:412–415.
23. Pipe JG. An optimized center-out k-space trajectory for multishot MRI: comparison with spiral and projection reconstruction. Magn Reson Med 1999;42:714–720.
24. Meyer C, Pauly JM, Nayak K, McConnell M, Macovski A, Nishimura DG, Hu BS. Real-time spiral SSFP cardiac imaging. In: Proceedings of the 9th Annual Meeting of ISMRM, Glasgow, Scotland, 2001. p 442.
25. Bornert P, Aldefeld B, Eggers H. Reversed spiral MR imaging. Magn Reson Med 2000;44:479–484.
26. Hargreaves BA, Meyer C, Yang P, Hu B, Nishimura D. Spiral SSFP coronary artery imaging. In: Proceedings of the 10th Annual Meeting of ISMRM, Honolulu, 2002. p 1589.
27. Irarrazabal P, Nishimura DG. Fast three-dimensional magnetic resonance imaging. Magn Reson Med 1995;33:656–662.
28. Bernstein MA, Licato PE. Angle-dependent utilization of gradient hardware for oblique MR imaging. J Magn Reson Imaging 1994;4:105–108.